Infrared Emitting and Photoconducting Colloidal Silver Chalcogenide Nanocrystal Quantum Dots from a Silylamide-Promoted Synthesis

Maksym Yarema,[†,*] Stefan Pichler,[†] Mykhailo Sytnyk,[†,‡] Robert Seyrkammer,[†] Rainer T. Lechner,[§] Gerhard Fritz-Popovski,[§] Dorota Jarzab,[⊥] Krisztina Szendrei,[⊥] Roland Resel,[•] Oleksandra Korovyanko,[‡] Maria Antonietta Loi,[⊥] Oskar Paris,[§] Günter Hesser,[×] and Wolfgang Heiss[†,*]

[†]Institute for Semiconductor and Solid State Physics, University Linz, Altenbergerstr. 69, Linz 4040, Austria, [‡]Department of Inorganic Chemistry, University Chernivtsi, L. Ukrainky Str. 25, Chernivtsi, 58012, Ukraine, [§]Institute of Physics, Montanuniversitaet Leoben, Franz Josef Str. 18, Leoben, 8700, Austria, [⊥]Zernike Institute for Advanced Materials, University of Groningen, Nijenborgh 4, Groningen 9747 AG, The Netherlands, [•]Institute of Solid State Physics, Graz University of Technology, Petersgasse 16, Graz 8010, Austria, and [×]Center of Surface and Nanoanalytics, University Linz, Altenbergerstr. 69, Linz 4040, Austria

ABSTRACT Here, we present a hot injection synthesis of colloidal Ag chalcogenide nanocrystals (Ag_2Se, Ag_2Te, and Ag_2S) that resulted in exceptionally small nanocrystal sizes in the range between 2 and 4 nm. Ag chalcogenide nanocrystals exhibit band gap energies within the near-infrared spectral region, making these materials promising as environmentally benign alternatives to established infrared active nanocrystals containing toxic metals such as Hg, Cd, and Pb. We present Ag_2Se nanocrystals in detail, giving size-tunable luminescence with quantum yields above 1.7%. The luminescence, with a decay time on the order of 130 ns, was shown to improve due to the growth of a monolayer thick ZnSe shell. Photoconductivity with a quantum efficiency of 27% was achieved by blending the Ag_2Se nanocrystals with a soluble fullerene derivative. The co-injection of lithium silylamide was found to be crucial to the synthesis of Ag chalcogenide nanocrystals, which drastically increased their nucleation rate even at relatively low growth temperatures. Because the same observation was made for the nucleation of Cd chalcogenide nanocrystals, we conclude that the addition of lithium silylamide might generally promote wet-chemical synthesis of metal chalcogenide nanocrystals, including in as-yet unexplored materials.

KEYWORDS: silver chalcogenides · semiconductor colloidal nanocrystals · photoconductivity · infrared emission · silylamide-promoted synthesis

Interesting perspectives on colloidal nanocrystal quantum dots (NCs) for infrared applications[1,2] were first demonstrated with PbS- and HgTe-based ultrasensitive photodetectors[3,4] and photodiodes,[5] as well as with CdTe/CdSe core/shell NCs with a staggered type-II band alignment,[6] which were applied as luminescence labels for cancer detection.[7] While the performance of NC-based devices are competitive with those based on epitaxial semiconductor heterostructures,[3,4] the potential for more environmentally benign alternatives for infrared active nanocrystal materials is currently being explored in order to avoid the use of the heavy metals Pb, Hg, or Cd. Such attempts include, for example, the synthesis of Bi or Sn chalcogenides,[8,9] of InAs-based NCs,[10,11] of Cu_2Se,[12] and $CuInS_2$[13] compounds, and here we introduce a relatively unexplored class: silver chalcogenide (Ag_2X, X = S, Se, Te) NCs.

Ag_2Xs exhibit different crystal structures, dependent on growth conditions and temperature. In their low-temperature structure, referred to here as β-phase, Ag_2Xs represent narrow band gap semiconductors with fundamental absorption edges at 0.15 eV for Ag_2Se, 0.67 eV for Ag_2Te, and 0.85 eV for Ag_2S.[14,15] Thus, heterostructures of Ag_2Xs are candidates for applications in infrared optical devices operating at wavelengths covering the telecommunication spectral regions as well as the technologically important atmospheric windows in the mid-infrared region. In addition, slight deviations from stoichiometric compositions in bulk Ag_2Te and Ag_2Se cause large magnetoresistance effects in these materials,[16,17] making them applicable also as megagauss sensors.[18] Due to these appealing properties of bulk Ag_2Xs, several attempts to obtain these materials in the form of colloidal NCs have been reported.[19−26]

With respect to the infrared activity of Ag_2Xs, pioneering work has been performed by the Murray group, who demonstrated an excitonic absorption peak at about 1.15 μm wavelength for monodisperse Ag_2Te NCs

* Address correspondence to wolfgang.heiss@jku.at, maksym.yarema@jku.at.

Received for review January 11, 2011 and accepted April 18, 2011.

Published online April 18, 2011
10.1021/nn2001118

with a size of 3 nm.[27] In addition, the Alivisatos group reported on size-tunable photoluminescence in the wavelength region between 1 and 1.3 μm from Ag_2S nanosegments, periodically embedded in CdS nanorods.[28] In this paper, we report on the demonstration of the infrared optical response of Ag_2Se NCs, which we believe has never been investigated for infrared absorption or emission. We show size-tunable photoluminescence (PL) for exceptionally small Ag_2Se NCs, with quantum yields above 1.7% and a decay time around 130 ns. While applying a ZnSe shell improves the emission intensity, blending the Ag_2Se NCs with a fullerene derivative allows the observation of photoconductivity with relatively high quantum efficiency. The described wet-chemical synthesis route greatly benefits from the addition of lithium silylamide, resulting in an increased NC nucleation. The generality of this approach is shown by the synthesis of further infrared active NCs, such as Ag_2Te and Ag_2S, as well as high-quality CdTe and CdSe with bright luminescence in the visible range.

RESULTS AND DISCUSSION

Ag_2Se Nanocrystal Synthesis. The published synthetic strategies regarding Ag_2Se-based spherical NCs of different quality include transformation from CdSe or ZnS NCs by complete cation exchange,[19,20] the treatment of Ag NCs by Se,[21] a positive microemulsion method,[22,23] and double jet precipitation.[22] Ag_2Se nanowires have also been demonstrated, synthesized by template-engaged synthesis strategies.[24−26] Although Ag_2Se NCs with orthorhombic crystal structure (low-temperature β-phase) as well as cubic crystal structure (high-temperature α-phase) have been obtained, to date, no infrared optical activity has been reported. We studied quantities such as photoluminescence quantum yield, luminescence decay time, and quantum efficiency in photoconductivity as a measure for the quality of the obtained semiconductor NCs and in order to test their potential for applications in infrared optical devices. The latter are of importance because Ag-based NCs can be expected to cause less environmental impact than the NC materials currently used in infrared optical devices, which contain toxic heavy metals.

As a general trend, a decrease of photoluminescence intensity with increasing size is observed in all infrared emitting NCs.[29−31] Therefore, to obtain photoluminescent Ag_2Se NCs, we developed a novel solution phase synthesis that resulted in especially small NC sizes. In our preliminary experiments, we followed the recently suggested concept of a quasi-seeded growth by cation exchange-mediated nucleation. This concept was demonstrated for PbSe NCs making use of SnSe intermediate nuclei.[29] In fact, the proposed mechanism was developed following the observed correlation

$$CF_3COOAg + Li[N(SiMe_3)_2] \rightleftharpoons \{Ag[N(SiMe_3)_2]\} + CF_3COOLi$$

$$\{Ag[N(SiMe_3)_2]\} \xrightarrow[\text{-byproducts}]{\text{in OLA}} [Ag^0] \xrightarrow{+TOPX} Ag_2X$$

Scheme 1. Proposed mechanism of Ag chalcogenide nanocrystal formation.

between final NC size and concentration of the applied Sn precursor, tin(II) bis[bis(trimethylsilyl)amide], ($Sn[N(SiMe_3)_2]_2$). For Ag_2Se NCs, we adapted the given recipe for PbSe NCs by replacing the Pb precursor with an appropriate Ag precursor, in our case, silver(I) trifluoroacetate (AgTFA). Oleylamine (OLA) was used as a coordinating solvent and trioctylphospine selenide (TOPSe) as the Se source. To guarantee that the obtained NCs exhibited the orthorhombic crystal structure (low-temperature modification), we restricted the nucleation temperature to values below 100 °C. Within this temperature limit, a direct reaction between AgTFA and TOPSe showed only a very slow nucleation after injection, and eventually very large Ag_2Se particles were obtained (Figure S1 in Supporting Information), likely due to insufficient reactivity of the precursors. However, the co-injection of $Sn[N(SiMe_3)_2]_2$, the precursor used for the formation of SnSe seeds,[29] together with the TOPSe resulted in an instantaneous nucleation and growth of Ag_2Se NCs. These NCs exhibit photoluminescence with a peak at 1060 nm, which is red-shifted with respect to the absorption edge found at 770 nm (Figure S2). Even though the chosen synthesis route appears to be successful, in that luminescent Ag_2Se NCs were achieved, the underlying mechanism seems to differ from that reported for PbSe.[29] In contrast to the case of PbSe, for the Ag_2Se NCs, the amount of $Sn[N(SiMe_3)_2]_2$ does not influence the final size of the obtained NCs. The NC size depends neither on reaction temperature, varied between room temperature and 100 °C, nor on growth time.

In order to cross-check these observations, we repeated the synthesis by replacing the $Sn[N(SiMe_3)_2]_2$ with another highly reactive silylamide. Specifically, with lithium bis(trimethylsilyl)amide ($Li[N(SiMe_3)_2]$), Ag_2Se NCs were also obtained, excluding the relevance of any cation exchange processes from SnSe nuclei for the present synthesis. Moreover, the Ag_2Se NCs obtained by the addition of $Li[N(SiMe_3)_2]$ outperformed even those obtained with $Sn[N(SiMe_3)_2]_2$ with respect to colloidal stability, photoluminescence quantum efficiency, and synthesis yield, typically found to range between 70 and 90%.[32] We thus conclude that the presence of the silylamide $[N(SiMe_3)_2]$ groups is the essential factor in speeding up the nucleation rate of this synthesis process. In particular, we suggest that the Ag_2Se NC synthesis follows a route as sketched in Scheme 1.

In the first step, a metathesis reaction between the silver salt (AgTFA) and the lithium silylamide results in the generation of short-lived silver silylamide complexes, depicted as $\{Ag[N(SiMe_3)_2]\}$ in Scheme 1. The

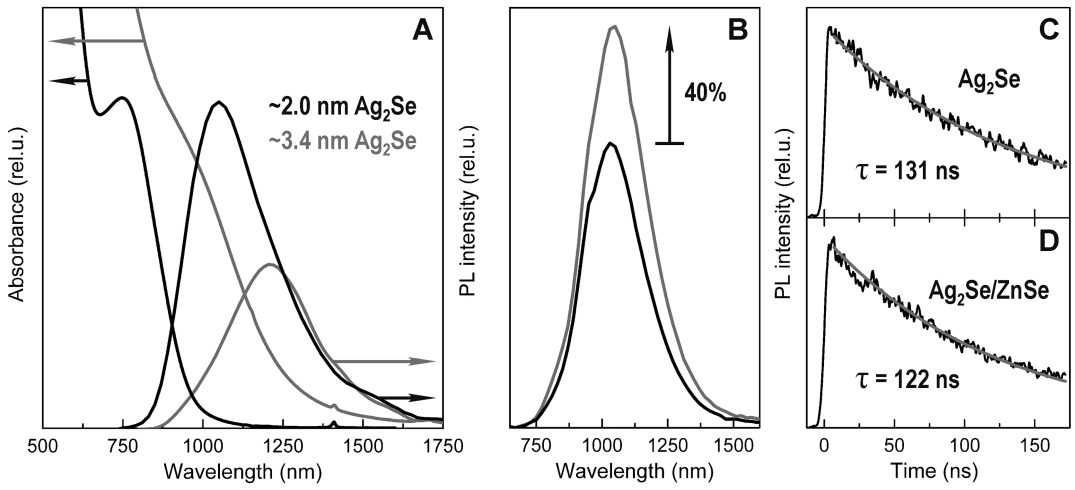

Figure 1. (A) Absorbance and emission spectra for Ag_2Se nanocrystals, 2.0 nm (black lines) and 3.4 nm in size (gray lines). (B) Emission spectra of 2.0 nm Ag_2Se (black line) and the same nanocrystals covered with a ZnSe shell (gray line). Time-resolved photoluminescence (black lines) of (C) 2.0 nm Ag_2Se nanocrystals and (D) Ag_2Se/ZnSe core/shell nanocrystals, presented together with exponential fits (gray lines).

subsequent decomposition of these silver silylamide complexes provides active silver centers [Ag^0], which instantly react with TOPSe to form Ag_2Se NCs. This overall scheme takes into account the following considerations: (i) The metathesis reaction between AgTFA and $Li[N(SiMe_3)_2]$ is driven by the higher ionization potential of silver (I_1(Ag) = 731 kJ·mol^{-1}) as compared to that of lithium (I_1(Li) = 520.2 kJ·mol^{-1}).[33] This difference in ionization potential results in a more favorable coordination of silver by $N(SiMe_3)_2$ groups in solution; in other words, the creation of covalent Ag−N bonds results in less dissociative silver silylamide. In addition, the subsequent decomposition of the silver silylamide complex ensures the irreversibility of this process. (ii) The metathesis reaction suggested above is supported by the similar reaction between potassium silylamide and silver chloride previously used to *ex situ* synthesize silver silylamide as bulk crystals.[34] This *ex situ* synthesized bulk silver silylamide has a tetramer crystal structure $\{Ag[\mu\text{-}N(SiMe_3)_2]_2\}_4$ and is thermally robust up to its melting point at approximately 275 °C. However, it cannot be used as Ag precursor in our synthesis because, surprisingly, it is insoluble in hydrocarbons.[35] (iii) The decomposition of the silver silylamide to silver in oleylamine environment is plausible because attempts to solve the bulk ($\{Ag[\mu\text{-}N(SiMe_3)_2]_2\}_4$) in hot tetrahydrofuran or pyridine have resulted in its decomposition to silver.[35] (iv) The tendency of silylamides to thermally decompose has been observed for several other silylamides, and it has actually been used for the synthesis of elemental Pb, Bi, and Ge NCs.[36−38] (v) The hypothesis that the reaction between silylamide derivatives and TOP chalcogens includes reduction to active metal centers as intermediate species was originally proposed by Polking *et al.*, who described the synthesis of GeTe.[38] We proved this hypothesis by performing a synthesis identical to that of Ag_2Se NCs, but without the addition of Se, resulting in metallic Ag NCs. These are easily identified by a narrow absorption peak found at 410 nm, due to the well-known plasmon resonance of Ag NCs at this wavelength[39] as well as by energy-dispersive X-ray spectroscopy (Figure S3 in Supporting Information). (vi) The reaction of TOPSe with Ag to Ag_2Se NCs is not surprising because the strategy of treating synthesized Ag NCs by chalcogens in order to obtain Ag_2X NCs has been reported previously.[21]

In the present synthesis of Ag_2Se NCs, the processes described in Scheme 1 are very fast and result therefore in exceptionally small sizes of NCs, in the range between 2 and 4 nm, as will be shown.

The Ag_2Se NCs obtained by the co-injection of lithium silylamide exhibit excitonic absorption features in the near-infrared region (Figure 1A), which can be tuned by size. For 2.0 nm Ag_2Se NCs, an excitonic absorption peak is observed close to 750 nm, while 3.4 nm NCs exhibit a shoulder at 1000 nm and an absorption onset at 1300 nm. The size of the NCs is mainly controlled by the Se to Ag ratio while increasing the growth time even results in a size focusing (Figures S4 and S5 in Supporting Information). For both sizes of NCs, luminescence can also be observed, with maxima at 1030 and 1250 nm, respectively. Thus there is a considerable Stokes shift on the order of 200 nm for both NC sizes, indicating the presence of (surface) defects, which also restrict the quantum yield, measured at 1.76% for the 2.0 nm Ag_2Se NCs. With increasing NC size, the intensity decreases, which is also observed for all other NC systems with infrared emission.[29−31] The situation can be improved by growing an inorganic shell around the Ag_2Se cores. To accomplish this, we injected zinc acetate solved in oleylamine into the as-grown Ag_2Se NC solution, containing an excess of Se, to obtain the ZnSe shell. ZnSe

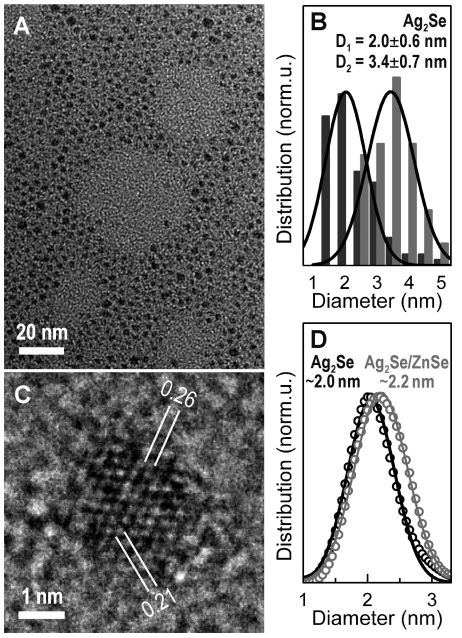

Figure 2. (A) TEM overview image of Ag_2Se nanocrystals. (B) Size histograms as deduced from TEM images fitted by Gauss distributions, for two differently sized nanocrystal batches, (C) High-resolution TEM image of a single Ag_2Se nanocrystal viewed in the [012] direction. (D) Distribution function of Ag_2Se nanocrystals before (black) and after (gray) growth of a ZnSe shell, as deduced from SAXS experiments (Figure S11 in Supporting Information).

was chosen due to (i) its high band gap energy as compared to that of Ag_2Se, resulting in a type-I band alignment between core and shell; (ii) its low toxicity; and (iii) its chemical robustness. Even though there is a considerable mismatch between the lattices of ZnSe (zinc blende structure with a lattice constant $a = 5.668$ Å) and Ag_2Se (orthorhombic crystal structure with a = 4.337, b = 7.070, c = 7.773 Å),[40] applying a ZnSe shell increases the PL intensity by up to 40% (Figure 1B). The Ag_2Se/ZnSe core/shell structure is also more stable than the core-only Ag_2Se NCs, and after a storing time of 6 months, the difference between PL intensities increases to a ratio of 5:1 (Figure S6). Growing a ZnSe shell results in a small red shift of the luminescence (Figure 1B), which is associated with the overall increase of the NC size. The PL decay time is only slightly affected: under 150 fs pulsed excitation, an almost monoexponential decay is observed with a characteristic decay time of 131 ns for the Ag_2Se core-only NCs and of 122 ns for the Ag_2Se/ZnSe core/shell NCs (Figure 1C,D). Both decay times are smaller than those observed with the same setup for the established infrared active NC materials PbS (2800 ns) and PbSe (1200 ns). However, the decay time is longer than for HgTe NCs (70 ns), which are well-known for their high quantum yields in both PL and photoconductivity experiments. Due to this lifetime, Ag_2Se might also be a promising candidate for photoconducting devices.[4,31]

The sizes and size distributions of the NCs were determined from overview images taken by transmission electron microscopy (TEM). Figure 2A shows a typical image achieved from the smallest Ag_2Se NCs. To obtain size histograms, at least 100 individual NCs were analyzed. Figure 2B shows size histograms from two batches with mean sizes of 2.0 ± 0.6 and 3.4 ± 0.7 nm, as determined from Gauss fits. Compared to previously reported Ag_2Se NCs, these obtained NCs are exceptionally small. The crystal structure of the NCs is determined by the indexing of selected area electron diffraction (SAED) rings (Figure S7 in Supporting Information), which confirmed that the NCs are Ag_2Se in its low-temperature β-modification ($P2_12_12_1$ structure group). This is also proven by the high-resolution TEM image in Figure 2C, showing an approximately 2.5 nm large NC oriented in the [012] direction and by the fact that the deduced lattice constants are in accordance with those expected for β-type Ag_2Se (a model NC of the same orientation is presented in Figure S8 of the Supporting Information). Furthermore, the composition of the Ag_2Se and Ag_2Se/ZnSe core/shell NCs is proven by energy-dispersive X-ray spectroscopy (Figure S9), confirming the expected 2 to 1 ratio between the Ag and Se, respectively, and a shell thickness corresponding to approximately 1 monolayer of ZnSe around the Ag_2Se NCs. The small NC sizes and their low crystal symmetry inhibit an accurate determination of their lattice parameters by wide-angle X-ray scattering (WAXS). The WAXS spectrum of the Ag_2Se NCs shows only a broad peak between 2θ angles of 30 and 45°, due to the overlap of a number of size broadened diffraction peaks (Figure S10).

Small-angle X-ray scattering (SAXS) analysis (Figure S11 in Supporting Information) provides accurate measures of size distributions of large ensembles of NCs. In particular, for the smallest Ag_2Se NCs, the size distribution function (see Figure 2D), weighted by particle volume as computed by generalized indirect Fourier transformation,[41] shows a NC diameter of 2.0 nm and a standard deviation of 19%. When the same analysis is applied after the growth of a ZnSe shell, a mean size of 2.2 nm is obtained, directly proving the crystallization of ZnSe on the Ag_2Se NC surface, similar to what has been reported for CdSe/ZnSe NCs.[42] In the distribution functions shown in Figure 2D, the scattering length contrast between Ag_2Se and ZnSe is not considered but can be taken into account by fitting the raw SAXS scattering curves by means of the GIFT-NG software with a spherical core, or core/shell model. From the data shown in Figure S11, we derive an Ag_2Se core diameter of 1.92 nm and a shell thickness of 0.22 nm. This results in a total outer diameter of the Ag_2Se/ZnSe NCs of 2.4 nm and a size distribution of 22%.

Ag_2Se Nanocrystals as Sensitizers in Photodetectors. Most importantly, the obtained NCs are useful in infrared optical devices, such as photodetectors. To obtain photoconductivity in NC assemblies, two strategies

were employed. Photoconductivity can be obtained (i) by manipulating the NC ligand shell in order to decrease the average NC distance in the film and thus increasing conductivity,[3−5,8] or (ii) by forming donor/acceptor type bulk heterojunctions providing charge separation within the film as well as sufficient charge transport channels for electrons and holes.[43] The latter approach has the advantage that the protecting ligand shell is fully restored, resulting in a higher stability in air, as compared to the ligand-manipulated NC layers. Such a donor/acceptor heterojunction is achieved by blending the Ag_2Se NCs with PCBM ([6,6]-phenyl-C_{61}-butyric acid methyl ester), a soluble derivative of C_{60}. The PCBM usually acts as efficient electron acceptor, assuming that the work function of the NCs is smaller than that of the PCBM (of approximately 4.3 eV).[44] The efficiency of the photoconducting device is also increased by the addition of the PCBM because the electron mobility in the PCBM is superior to that typically observed in NC films. To measure the photoconductivity, a blend with a weight ratio of 1:4 Ag_2Se NCs/PCBM solved in chlorobenzene is drop-casted onto interdigitated gold electrodes with a distance of 20 μm and an active area of 13.5 mm^2, fabricated on glass substrates. The photosensitivity of this blend is evidenced by the current/voltage characteristics, showing a 7.3 times current increase under 4 mW/cm^2 illumination with a broad-band infrared light source (λ > 850 nm, Figure 3A). That this photosensitivity is caused by absorption only in the Ag_2Se NCs is evidenced by the fact that the measured response is observed at wavelengths well below the absorption onset of PCBM. The latter is found at a wavelength of 750 nm in absorbance as well as in photoconductivity (Figure S12 in Supporting Information). Thus the responsivity spectrum in Figure 3B, starting at a wavelength of 900 nm, is also caused solely by absorbance in the Ag_2Se NCs. At this wavelength, the responsivity amounts to 0.2 A/W, corresponding to a quantum efficiency of 27%. While this value is not as good as those reported for PbS/PCBM blends measured under identical conditions,[43] further optimizations are possible. With the Ag_2Se NCs/PCBM blends, a photoresponse is obtained up to a wavelength of 1300 nm (Figure 3B). This wavelength is somewhat longer than the cutoff wavelength of standard photodetectors based on crystalline silicon, and it is within the spectral region of minimum absorbance of human tissues and blood, so that biomedical applications of Ag_2Se NC detectors could be feasible.

Other Ag Chalcogenide Nanocrystals and Generality of the Silylamide-Promoted Synthesis. As shown in Scheme 1, the described synthesis route is not necessarily restricted to selenides but might also be applicable to tellurides and sulfides. In fact, both Ag_2S and Ag_2Te could be obtained by replacing TOPSe with the corresponding TOPX. The absorption and PL spectrum of 3.1 nm Ag_2S

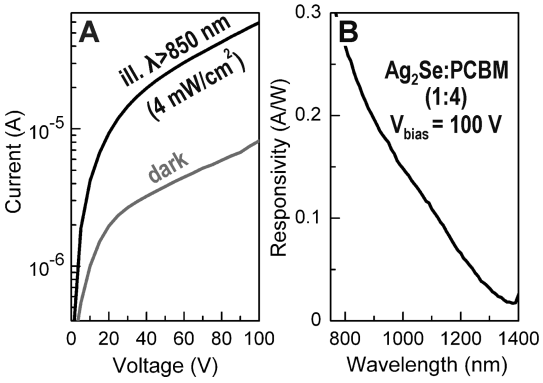

Figure 3. (A) *I*−*V* characteristics of a Ag_2Se nanocrystal/PCBM blend under illumination (black line) and in dark (gray line). (B) Photoresponsivity spectrum of the same blend.

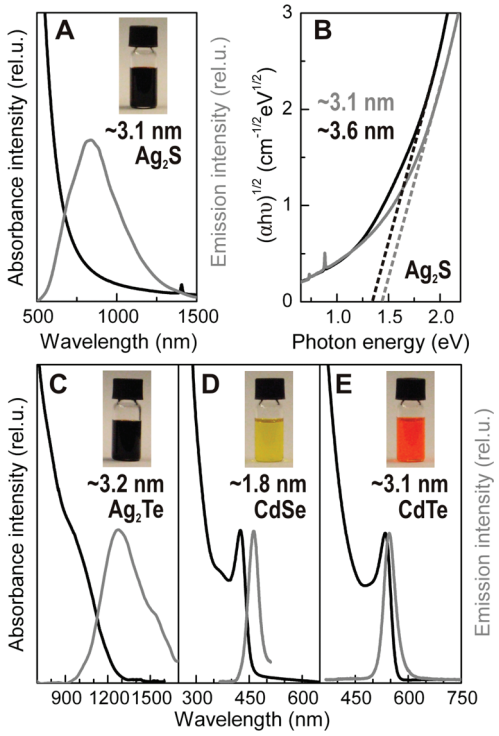

Figure 4. Absorption and emission spectra for Ag_2S nanocrystals on linear scale (A), and on a scale appropriate for the application of Bardeen or Tauc equation to deduce the indirect band gap energy (B). Absorption and emission spectra of (C) Ag_2Te, (D) CdSe, and (E) CdTe nanocrystals, synthesized *via* silylamide-promoted synthesis (linear scale).

are shown in Figure 4A. The energy band gaps (E_g) of 3.1 and 3.6 nm Ag_2S NCs, deduced *via* the Bardeen or Tauc equation,[45,46] are found at approximately 1.45 and 1.35 eV, respectively. As expected, the band gap energies are increased with respect to that of bulk material (0.85 eV),[14] in contrast to what has previously been reported for larger sized Ag_2S NCs.[45] Ag_2Te NCs are also obtained, and for 3.2 nm large NCs, photoluminescence is found to peak at 1300 nm and to reach up to 1500 nm (Figure 4C). The photoluminescence from Ag_2Te NCs has not been previously reported and

thus represents a novel materials system with potential for further applications in infrared devices. EDX spectra show the expected 2:1 Ag/Te ratio for the Ag_2Te NCs, whereas for the Ag_2S sample, an excess of Ag is detected (Figure S13 in Supporting Information). This might be caused by the low reactivity of TOPS, resulting in a mixture of Ag and Ag_2S NCs in the sample. The sizes of the Ag_2S and Ag_2Te NCs shown in Figure 4 were deduced from the TEM images in Figures S14 and S15.

Since lithium has very low ionization energy, the lithium-silylamide-promoted synthesis could serve as general route toward metal chalcogenide NCs. We have also obtained good results for CdSe and CdTe NCs, as shown in Figure 4D,E. Their diameters were deduced from their optical transition energies by using an experimentally derived sizing formula reported by Yu *et al.*[47] Furthermore, we performed successful synthesis with the same scheme for ZnSe, MnSe, PbSe, and Cu_2Se, proving that the *in situ* synthesis of metal silylamides is a powerful strategy for the one-pot synthesis of a large class of small sized chalcogenide NCs, including as-yet unexplored materials.

CONCLUSIONS

We demonstrated a high-yield wet-chemical synthesis of 2.0 to 3.4 nm β-type Ag_2Se NCs, with a size control given by the Ag to Se precursor ratio. The optical absorbance and photoluminescence spectra in the infrared region reveal strong confinement effects. While the growth of a ZnSe shell is proven to enhance the photoluminescence intensity, mixing the NCs with a fullerene results in photoconductivity signals up to a wavelength of 1200 nm. Due to the low toxicity of these materials, the Ag_2Se/ZnSe core/shell NCs might be used as an alternative to the standard infrared materials containing heavy metals such as Pb, Cd, and Hg. We found that a key to the synthesis of such small Ag_2Se NCs is the co-injection of a highly reactive silylamide, and we applied the same synthesis route to the synthesis of Ag_2Te, Ag_2S, and other nanocrystal materials, demonstrating the generality of this approach.

EXPERIMENTAL SECTION

Materials. Silver(I) trifluoroacetate (AgTFA, 98%), tin(II) bis[bis(trimethylsilyl)amide] ($Sn[N(SiMe_3)_2]_2$), lithium bis(trimethylsilyl)amide ($Li[N(SiMe_3)_2]$, 97%), oleic acid (OA, 90%), sulfur (99.998%), tellurium (99.99%), zinc acetate ($Zn(Ac)_2$, 99.99%), cadmium(II) chloride (99.99+%), lead(II) oxide (99.999%), hexamethyldisilathiane (purum grade), octadecene (90%, techn.), chloroform (≥99.8%), toluene (≥99.9%), tetrachloroethylene (≥99.9%), hexane (≥97%), ethanol, and methanol were purchased from Sigma-Aldrich; tri-*n*-octylphosphine (TOP, 97%) from Strem; selenium (99.999%) from Alfa Aesar; oleylamine (OLA, 80−90%) from Acros. All were used without previous purification. The 10% (w/w) solutions of selenium or tellurium in TOP (TOPSe and TOPTe, respectively) and 5% (w/w) of sulfur (TOPS) were prepared by dissolving the appropriate amounts of chalcogens in TOP under N_2 atmosphere.

Synthesis of Ag_2Se Nanocrystals. All syntheses were carried out under oxygen-free and dry atmosphere using standard Schlenk-line technique. A recipe to produce the smallest (2.0 nm in size) Ag_2Se NCs is given below.

AgTFA (1 mmol) and OLA (10 mL) were heated up to 70 °C for dissolving and purification under vacuum for 1 h and then flushed with argon for 30 min. $Li[N(SiMe_3)_2]$ (0.4 g) was dissolved in 10% (w/w) TOPSe (2.5 mL) with sonication and then swiftly injected. The reaction was continued for 1 h at constant temperature. After cooling, the NCs were isolated by adding a chloroform/methanol mixture and by centrifugation. The nonpolar/polar washing procedure was repeated once, and the NCs were then solved in a common nonpolar solvent.

The average size of the produced NCs can be well controlled by the ratio between Se and Ag precursors (Figure S4 in Supporting Information). The reaction was tested in a temperature range between room temperature and 100 °C. The time of reaction is highly temperature dependent and lasts from 2 min to several days in order to achieve the optimal size dispersivity. The amount of silylamide does not essentially influence the final size of the NCs.

Synthesis of Ag_2Se/ZnSe Core/Shell Nanocrystals. $Zn(Ac)_2$ (1.5 mmol) was dissolved in dried OLA (5 mL) inside a glovebox by heating it to 100 °C for 1 h. The obtained zinc precursor was injected into an Ag_2Se NC solution, synthesized at 70 °C according to the procedure described above, and the temperature was kept constant for another 1 h. The NCs were cooled to RT and washed twice with a chloroform/methanol mixture and centrifugation, and then some amount of OA was added to improve the colloidal stability. The amount of 0.3 M Zn acetate solution (in OLA) was calculated to be equimolar to the Se excess, still remaining after Ag_2Se NC synthesis.

Syntheses of Other Materials. The Ag_2Te, Ag_2S, CdSe, and CdTe NCs were synthesized similarly to Ag_2Se, taking appropriate TOP chalcogenides and adjusting the reaction temperature.

Characterization of Nanocrystals. Linear absorption spectra were taken using a JASCO V670 spectrometer operating from 200 to 2700 nm. TEM and HRTEM images and electron diffraction patterns were obtained using JEOL 2011 FasTEM microscope operating at an accelerated voltage of 200 kV. EDX elemental were performed on a JEOL JSM-6400 SEM microscope. X-ray diffraction patterns were collected with a Siemens D501 powder diffractometer operating in Bragg−Brentano focusing geometry using Cu Kα radiation (1.5406 Å) and a graphite monochromator on the secondary side. Small-angle scattering (SAXS) data were measured using synchrotron radiation at the μ-Spot beamline of the BESSY II storage ring (Helmholtz Zentrum Berlin fuer Materialien and Energie). Data were recorded with a 2D detector using the standard SAXS setup[48] at an X-ray energy of 15 keV.

The excitation source for the photoluminescence measurements was a Spectra Physics continuous wave argon ion laser, model 163A 5216, emitting at a wavelength of 514 nm. The maximum emission power of 50 mW was utilized for the experiments. The exciting beam was chopped by a chopper wheel and focused on the cuvettes containing the NCs in solution. The photoluminescence was collected by two CaF_2 lenses and spectrally resolved by an Acton Research Corporation Spectra Pro 150 monochromator. The monochromatic light was detected by a nitrogen-cooled Judson J10-M204-R10 M InSb photodiode. This signal was amplified with a Judson PA-7 preamplifier and a Stanford Research System SR510 lock-in amplifier, which used the excitation source chopper frequency

as a reference. A self-written program running on a personal computer operated the monochromator over the desired spectral range and evaluated the amplified signals at the different wavelengths to obtain the photoluminescence spectra. To quantify the efficiency, the incident and reflected laser power was measured and the luminescence was focused onto a high sensitivity pyrometer from Spectrum Detectors Inc. (STEP 49, calibrated by the National Institute of Standards and Technology (NIST)), placed in front of the entrance slit of the grating spectrometer. Losses at the lenses and the utilized RG 550 long path filter were taken into account. While the measurement collected the PL signal within a room angle of 0.236 sr, as given by the F-number of the collecting lens, the total emitted power was obtained by integration over a sphere.

Photoconductivity measurements were carried out using the same optical elements, spectrometer, and lock-in amplifier as was used for the PL experiments. The *I*—*V* characteristics were measured with a Keithley 236 Source Measure Unit, and for illumination, a 40 W halogen lamp was used. To measure the illumination power, a high sensitivity pyrometer from Spectrum Detectors Inc. (STEP 49) was used.

Time-resolved PL measurements were performed by exciting the samples at 774 nm with a Ti:sapphire laser that provided 150 fs pulses. The PL emission was detected using a spectrometer coupled to a Hamamatsu streak camera with a cathode sensitive to near-IR radiation.

Acknowledgment. The authors wish to thank the Austrian Science Fund FWF (Project SFB IR_ON) and the EU's seventh Framework Programme (FP7/2007-2013, No. 226716) for financial support, as well as Prof. G. Knör for allowing us to use his equipment for linear absorbance measurements. We are also thankful to Dr. U. Monkovius, S. Minniberger, O. Fuchs, E. Pachinger (University Linz), and B. Aichmayer, S. Siegel, and C. Li (MPI of Colloids and Interfaces in Potsdam) for technical support.

Supporting Information Available: Supporting Figures S1—S15 with descriptions. This material is available free of charge *via* the Internet at http://pubs.acs.org.

REFERENCES AND NOTES

1. Wehrenberg, B. L.; Wang, C.; Guyot-Sionnest, P. Interband and Intraband Optical Studies of PbSe Colloidal Quantum Dots. *J. Phys. Chem. B* **2002**, *106*, 10634–10640.
2. Rogach, A. L.; Eychmüller, A.; Hickey, S. G.; Kershaw, S. V. Infrared-Emitting Colloidal Nanocrystals: Synthesis, Assembly, Spectroscopy, and Applications. *Small* **2007**, *3*, 536–557.
3. Konstantatos, G.; Howard, I.; Fischer, A.; Hoogland, S.; Clifford, J.; Klem, E.; Levina, L.; Sargent, E. H. Ultrasensitive Solution-Cast Quantum Dot Photodetectors. *Nature* **2006**, *442*, 180–183.
4. Böberl, M.; Kovalenko, M.; Gamerith, S.; List, E.; Heiss, W. Inkjet-Printed Nanocrystal Photodetectors Operating up to 3 μm Wavelengths. *Adv. Mater.* **2007**, *19*, 3574–3578.
5. Clifford, J. P.; Konstantatos, G.; Johnston, K. W.; Hoogland, S.; Levina, L.; Sargent, E. H. Fast, Sensitive and Spectrally Tuneable Colloidal-Quantum-Dot Photodetectors. *Nat. Nanotechnol.* **2009**, *4*, 40–44.
6. Kim, S.; Fisher, B.; Eisler, H.-J.; Bawendi, M. Type-II Quantum Dots: CdTe/CdSe (Core/Shell) and CdSe/ZnTe (Core/Shell) Heterostructures. *J. Am. Chem. Soc.* **2003**, *125*, 11466–11467.
7. Kim, S.; Lim, Y. T.; Soltesz, E. G.; De Grand, A. M.; Lee, J.; Nakayama, A.; Parker, J. A.; Mihaljevic, T.; Laurence, R. G.; Dor, D. M.; *et al.* Near-Infrared Fluorescent Type II Quantum Dots for Sentinel Lymph Node Mapping. *Nat. Biotechnol.* **2004**, *22*, 93–97.
8. Konstantatos, G.; Levina, L.; Tang, J.; Sargent, E. H. Sensitive Solution-Processed Bi_2S_3 Nanocrystalline Photodetectors. *Nano Lett.* **2008**, *8*, 4002–4006.
9. Kovalenko, M. V.; Heiss, W.; Shevchenko, E. V.; Lee, J.-S.; Schwinghammer, H.; Alivisatos, A. P.; Talapin, D. V. SnTe Nanocrystals: A New Example of Narrow-Gap Semiconductor Quantum Dots. *J. Am. Chem. Soc.* **2007**, *129*, 11354–11355.
10. Cao, Y. W.; Banin, U. Growth and Properties of Semiconductor Core/Shell Nanocrystals with InAs Cores. *J. Am. Chem. Soc.* **2000**, *122*, 9692–9702.
11. Battaglia, D.; Peng, X. Formation of High Quality InP and InAs Nanocrystals in a Noncoordinating Solvent. *Nano Lett.* **2002**, *2*, 1027–1030.
12. Deka, S.; Genovese, A.; Zhang, Y.; Miszta, K.; Bertoni, G.; Krahne, R.; Giannini, C.; Manna, L. Phosphine-Free Synthesis of p-Type Copper(I) Selenide Nanocrystals in Hot Coordinating Solvents. *J. Am. Chem. Soc.* **2010**, *132*, 8912–8914.
13. Li, L.; Daou, T. J.; Texier, I.; Kim Chi, T. T.; Liem, N. Q.; Reiss, P. Highly Luminescent $CuInS_2$/ZnS Core/Shell Nanocrystals: Cadmium-Free Quantum Dots for *In Vivo* Imaging. *Chem. Mater.* **2009**, *21*, 2422–2429.
14. Junod, P.; Hediger, H.; Kilchör, B.; Wullschleger, J. Metal—Nonmetal Transition in Silver Chalcogenides. *Philos. Mag.* **1977**, *36*, 941–958.
15. Appel, J. Uber Elektrische und Optische Eigenschaften des Silbertellurids Ag_2Te. *Z. Naturforsch.* **1955**, *10a*, 530–537.
16. Boolchand, P.; Bresser, W. J. Mobile Silver Ions and Glass Formation in Solid Electrolytes. *Nature* **2001**, *410*, 1070–1073.
17. Xu, R.; Husmann, A.; Rosenbaum, T. F.; Saboungi, M. L.; Enderby, J. E.; Littlewood, P. B. Large Magnetoresistance in Non-magnetic Silver Chalcogenides. *Nature* **1997**, *390*, 57–60.
18. Husmann, A.; Betts, J. B.; Boebinger, G. S.; Migliori, A.; Rosenbaum, T. F.; Saboungi, M. L. Megagauss Sensors. *Nature* **2002**, *417*, 421–424.
19. Son, D. H.; Hughes, S. M.; Yin, Y.; Alivisatos, A. P. Cation Exchange Reactions in Ionic Nanocrystals. *Science* **2004**, *306*, 1009–1012.
20. Wang, S.-B.; Hu, B.; Liu, C.-C.; Yu, S.-H. Syringe Pump-Assisted Synthesis of Water-Soluble Cubic Structure Ag_2Se Nanocrystals by a Cation-Exchange Reaction. *J. Colloid Interface Sci.* **2008**, *325*, 351–355.
21. Wang, D.; Xie, T.; Peng, Q.; Li, Y. Ag, Ag_2S, and Ag_2Se Nanocrystals: Synthesis, Assembly, and Construction of Mesoporous Structures. *J. Am. Chem. Soc.* **2008**, *130*, 4016–4022.
22. Buschmann, V.; Van Tendeloo, G.; Monnoyer, P.; Nagy, J. B. Structural Characterization of Colloidal Ag_2Se Nanocrystals. *Langmuir* **1998**, *14*, 1528–1531.
23. Ge, J. P.; Xu, S.; Liu, L. P.; Li, Y. D. A Positive-Microemulsion Method for Preparing Nearly Uniform Ag_2Se Nanoparticles at Low Temperature. *Chem.—Eur. J.* **2006**, *12*, 3672–3677.
24. Wang, H.; Qi, L. Controlled Synthesis of Ag_2S, Ag_2Se, and Ag Nanofibers by Using a General Sacrificial Template and Their Application in Electronic Device Fabrication. *Adv. Funct. Mater.* **2008**, *18*, 1249–1256.
25. Zhang, S.-Y.; Fang, C.-X.; Wei; Jin, B.-K.; Tian, Y.-P.; Shen, Y.-H.; Yang, J.-X.; Gao, H.-W. Synthesis and Electrochemical Behavior of Crystalline Ag_2Se Nanotubes. *J. Phys. Chem. C* **2007**, *111*, 4168–4174.
26. Gates, B.; Mayers, B.; Wu, Y.; Sun, Y.; Cattle, B.; Yang, P.; Xia, Y. Synthesis and Characterization of Crystalline Ag_2Se Nanowires through a Template-Engaged Reaction at Room Temperature. *Adv. Funct. Mater.* **2002**, *12*, 679–686.
27. Urban, J. J.; Talapin, D. V.; Shevchenko, E. V.; Kagan, C. R.; Murray, C. B. Synergism in Binary Nanocrystal Superlattices Leads to Enhanced p-Type Conductivity in Self-Assembled PbTe/Ag_2Te Thin Films. *Nat. Mater.* **2007**, *6*, 115–121.
28. Robinson, R. D.; Sadtler, B.; Demchenko, D. O.; Erdonmez, C. K.; Wang, L.-W.; Alivisatos, A. P. Spontaneous Superlattice Formation in Nanorods through Partial Cation Exchange. *Science* **2007**, *317*, 355–358.
29. Kovalenko, M.; Talapin, D.; Loi, M.; Cordella, F.; Hesser, G.; Bodnarchuk, M.; Heiss, W. Quasi-Seeded Growth of Ligand-Tailored PbSe Nanocrystals through Cation-Exchange-Mediated Nucleation. *Angew. Chem., Int. Ed.* **2008**, *47*, 3029–3033.

30. Semonin, O. E.; Johnson, J. C.; Luther, J. M.; Midgett, A. G.; Nozik, A. J.; Beard, M. C. Absolute Photoluminescence Quantum Yields of IR-26 Dye, PbS, and PbSe Quantum Dots. *J. Phys. Chem. Lett.* **2010**, *1*, 2445–2450.
31. Kovalenko, M. V.; Kaufmann, E.; Pachinger, D.; Roither, J.; Huber, M.; Stangl, J.; Hesser, G.; Schäffler, F.; Heiss, W. Colloidal HgTe Nanocrystals with Widely Tunable Narrow Band Gap Energies: From Telecommunications to Molecular Vibrations. *J. Am. Chem. Soc.* **2006**, *128*, 3516–3517.
32. The amount of Ag_2Se NCs was roughly estimated from balancing the solid remains from NC solutions with well-defined volumes, taking into account the amount of ligands (TOP is assumed as ligand), as determined from EDX spectra. The yield is the ratio between Ag_2Se NCs obtained from the synthesis and total Ag_2Se amount as calculated from the AgTFA reaction (Scheme 1).
33. Lide, D. R. Ionization Potentials of Atoms and Atomic Ions. In *CRC Handbook of Chemistry and Physics*, 82nd ed.; Chemical Rubber Co. Press LLC: Boca Raton, FL, 2002; pp 10−175.
34. Bürger, H.; Seyffert, H. Bildung und Eigenschaften von Alkali-Disilylamiden. *Angew. Chem.* **1964**, *76*, 577–577.
35. Hitchcock, P. B.; Lappert, M. F.; Pierssens, L. J. M. Synthesis and X-ray Molecular Structures of the Silver(I) Amides $[\{Ag[\mu\text{-}N(SiMe_3)_2]\}_4]$ and $[\{Ag[\mu\text{-}NCMe_2(CH_2)_3CMe_2]\}_4]$. *Chem. Commun.* **1996**, 1189–1190.
36. Zolotavin, P.; Guyot-Sionnest, P. Meissner Effect in Colloidal Pb Nanoparticles. *ACS Nano* **2010**, *4*, 5599–5608.
37. Yarema, M.; Kovalenko, M. V.; Hesser, G.; Talapin, D. V.; Heiss, W. Highly Monodisperse Bismuth Nanoparticles and Their Three-Dimensional Superlattices. *J. Am. Chem. Soc.* **2010**, *132*, 15158–15159.
38. Polking, M. J.; Zheng, H.; Ramesh, R.; Alivisatos, A. P. Controlled Synthesis and Size-Dependent Polarization Domain Structure of Colloidal Germanium Telluride Nanocrystals. *J. Am. Chem. Soc.* **2011**, *133*, 2044–2047.
39. Jin, R.; Cao, Y.-W.; Mirkin, C. A.; Kelly, K. L.; Schatz, G. C.; Zheng, J. G. Photoinduced Conversion of Silver Nanospheres to Nanoprisms. *Science* **2001**, *294*, 1901–1903.
40. Billetter, H.; Ruschewitz, U. Structural Phase Transitions in Ag_2Se (Naumannite). *Z. Anorg. Allg. Chem.* **2008**, *634*, 241–246.
41. Glatter, O. Determination of Particle-Size Distribution Functions from Small-Angle Scattering Data by Means of the Indirect Transformation Method. *J. Appl. Crystallogr.* **1980**, *13*, 7–11.
42. Talapin, D. V.; Mekis, I.; Götzinger, S.; Kornowski, A.; Benson, O.; Weller, H. CdSe/CdS/ZnS and CdSe/ZnSe/ZnS Core−Shell−Shell Nanocrystals. *J. Phys. Chem. B* **2004**, *108*, 18826–18831.
43. Szendrei, K.; Cordella, F.; Kovalenko, M. V.; Böberl, M.; Hesser, G.; Yarema, M.; Jarzab, D.; Mikhnenko, O. V.; Gocalinska, A.; Saba, M.; *et al.* Solution-Processable Near-IR Photodetectors Based on Electron Transfer from PbS Nanocrystals to Fullerene Derivatives. *Adv. Mater.* **2009**, *21*, 683–687.
44. Soci, C.; Hwang, I. W.; Moses, D.; Zhu, Z.; Waller, D.; Gaudiana, R.; Brabec, C. J.; Heeger, A. J. Photoconductivity of a Low-Bandgap Conjugated Polymer. *Adv. Funct. Mater.* **2007**, *17*, 632–636.
45. Huxter, V. M.; Mirkovic, T.; Nair, P. S.; Scholes, G. D. Demonstration of Bulk Semiconductor Optical Properties in Processable Ag_2S and EuS Nanocrystalline Systems. *Adv. Mater.* **2008**, *20*, 2439–2443.
46. Anthony, S. P. Synthesis of Ag_2S and Ag_2Se Nanoparticles in Self Assembled Block Copolymer Micelles and Nano-Arrays Fabrication. *Mater. Lett.* **2009**, *63*, 773–776.
47. Yu, W. W.; Qu, L.; Guo, W.; Peng, X. Experimental Determination of the Extinction Coefficient of CdTe, CdSe, and CdS Nanocrystals. *Chem. Mater.* **2003**, *15*, 2854–2860.
48. Gourrier, A.; Wagermaier, W.; Burghammer, M.; Lammie, D.; Gupta, H. S.; Fratzl, P.; Riekel, C.; Wess, T. J.; Paris, O. Scanning X-ray Imaging with Small-Angle Scattering Contrast. *J. Appl. Crystallogr.* **2007**, *40*, 78–82.